QCD EFFECTS ON THE EVENT STRUCTURE
IN LEPTOPRODUCTION

M. BENGTSSON[a], G. INGELMAN[b], and T. SJÖSTRAND[a]

[a]*Department of Theoretical Physics, University of Lund, Sölvegatan 14A, S-223 62 Lund, Sweden*
[b]*Deutsches Elektronen-Synchrotron DESY, Notkestrasse 85, D-2000 Hamburg 52, FRG*

Perturbative QCD corrections to leptoproduction events can be introduced either in the form of matrix elements or of parton showers. Each of these approaches has its advantages and disadvantages, making a comparison of the two interesting. At present energies, both methods can be made to agree reasonably well with data, whereas differences appear at higher energies. The influence of these QCD effects on the expected event structure at ep colliders, HERA in particular, is investigated in detail. This includes multiplicity and momentum distributions, transverse momentum flow and correlations, as well as jet properties.

1. Introduction

Leptoproduction is one of the main fields of experimental high energy physics, with a program complementary to the ones offered by e^+e^- annihilation and hadron collisions. At present, new results are mainly provided by the fixed target programs at CERN and Fermilab. In a few years HERA is planned to offer ep collisions at 30 GeV on 820 GeV; a combination of LEP and LHC might give 95 GeV on 8.5 TeV. Studies at higher energies have two main objectives, to improve current understanding of the standard model and to look for signals for new physics. These studies will be based both on the overall kinematical variables and on the detailed event structure.

The two main kinematical variables, x and Q^2, can be calculated from a knowledge of incoming and scattered lepton momenta. For an incoming electron or muon beam, this procedure is straightforward in neutral current (γ/Z^0 exchange) events, but less so in charged current ($W^\pm$ exchange) ones, where the outgoing neutrino is not detected. If the hadronic system in the event can be measured, energy-momentum conservation gives the neutrino momentum, however. It then becomes a matter of understanding the detailed response of a detector, in particular degradations due to an imperfect angular coverage, which presupposes a knowledge of the structure of the hadronic system. Some of this knowledge, but not all, may come from a "calibration" in neutral current events, where both the scattered lepton

and the hadronic system may be observed. Also a more elaborate study of the event shape, e.g. a search for new particles decaying into several jets, or combinations of leptons and jets, must be based on some notion of what to expect from standard model backgrounds. Hence, it is important to have as well-founded expectations as possible for the event structure in very high energy leptoproduction.

The required understanding of hadron production is today not provided directly by QCD. Rather, a composite picture is used, wherein a perturbative treatment of parton production is combined with a nonperturbative model for the fragmentation of a partonic state into hadrons. In the latter capacity, the Lund string model [1] will be used throughout. For the perturbative part, two main alternatives are possible: matrix elements and parton showers. In principle, the former approach is superior, in that matrix elements involve no kinematical approximations and in that the complete structure in x and Q^2 is included. For fixed target energies, the matrix element route has already been proven phenomenologically viable [2–4]. However, experience with experiments at PETRA and PEP have taught us that not even second order matrix elements provide a satisfactory description of data at or above $W = 30$ GeV [5]. In particular, the amount of multijet events is underestimated, indicating a need for higher order corrections. It is therefore not to be expected that the matrix elements at our disposal in leptoproduction, which are of first rather than second order, should fare any better at the larger W-values probed with HERA. Parton showers are based on an iterative picture of successive branchings. Multiparton configurations are therefore generated in a natural fashion, resulting in an improved agreement with the multijet phenomenology in e^+e^- annihilation [5]. The parton shower approach should therefore also give a more realistic picture of the complexity of high energy leptoproduction events than that offered by first order matrix elements. Unfortunately, the parton shower algorithms include various kinematical simplifications, making the results particularly uncertain for the amount of hard emission.

The objective of the present paper is to compare the matrix element (ME) and parton shower (PS) approaches, in the context of currently available data as well as expectations for higher energies. These comparisons will be exclusively for standard model events – the not insignificant differences obtained between the two approaches is as good a motivation as any why the study of QCD phenomena should not be considered a finished chapter. The plan of the paper is as follows. A brief introduction to the simple quark parton model (QPM), without any QCD corrections, and its two extensions (ME and PS) is given in sect. 2. In sect. 3 it is shown that parton showers can be made to agree with data at present energies, as has already been shown for the ME approach by EMC [4,6], while the quark parton model fails. At higher energies differences will become even larger, in particular if phenomena sensitive to multijet emission are studied; sect. 4. The specific problem of kinematics reconstruction from the hadronic system (in charged current events) is briefly discussed in sect. 5. Finally, a summary and outlook is given in sect. 6.
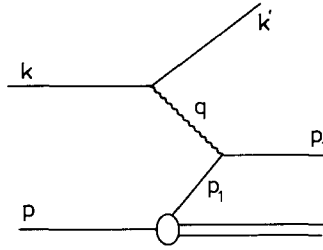
Fig. 1. Kinematics notation for the naive parton model, i.e. without any QCD corrections. Particles that appear "after" the boson exchange are always written with a prime. The proton four-momentum is denoted by capital P.

2. The models

The kinematics of leptoproduction, fig. 1, is given in terms of the four-momenta k and k' of the incoming and outgoing lepton and the nucleon target momentum vector P. The momentum of the exchanged electroweak current, $q = k - k'$, is a spacelike vector, i.e. $q^2 = -Q^2$, $Q^2 > 0$. A commonly used variable is ν, defined by the relation $m_p\nu = P \cdot q$, i.e. the energy of the current in the target rest frame. The scaling variables are given by

$$x \equiv \frac{Q^2}{2P \cdot q} = \frac{Q^2}{2m_p\nu}, \tag{1}$$

$$y \equiv \frac{P \cdot q}{P \cdot k} = \frac{2P \cdot q}{s} = \frac{\nu}{\nu_{max}}, \tag{2}$$

where $s = (P + k)^2$ is the total invariant mass-squared. We note that the identification of x as the momentum fraction of the incoming quark, i.e. $p = xP$, is only correct for a scattering of massless partons – a condition which will normally not be fulfilled in QCD processes, where off-shell partons may occur. The invariant mass of the hadronic final state, which is an important variable both for perturbative QCD and hadronization, is given by

$$W^2 \equiv (P + q)^2 = Q^2\frac{1 - x}{x} + m_p^2. \tag{3}$$

The deep inelastic scattering cross section can be well illustrated by that of the purely electromagnetic interaction, i.e. photon exchange,

$$\frac{d^2\sigma}{dx\, dQ^2} = \frac{2\pi\alpha^2}{xQ^4}\left\{1 + (1 - y)^2\right\} \sum_{i=q,\bar{q}} e_i^2 x f_i(x, Q^2), \tag{4}$$
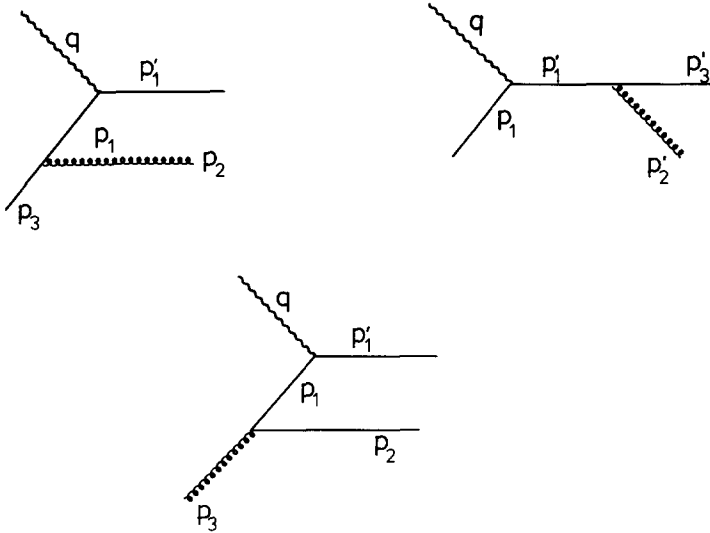
Fig. 2. The first order QCD processes, gluon radiation and boson-gluon fusion, giving the lowest order corrections to the basic process in fig. 1.

where f_i is the structure function for a quark of flavour i with electric charge e_i. The same basic structure holds also for the weak processes, but with other Q^2-dependent propagators, y-dependent helicity factors and flavour couplings. QCD corrections are included through the Q^2 dependence of the structure functions. QED radiative corrections, in particular photon bremsstrahlung off the incoming lepton, introduce further complications. These are not considered in the present paper, since they are normally corrected for in the experimental data.

The lowest order (QPM) partonic process $\gamma^* + q \rightarrow q$ is in first order QCD supplemented by gluon radiation and boson-gluon fusion, $\gamma^* + q \rightarrow q + g$ and $\gamma^* + g \rightarrow q + \bar{q}$, as shown in fig. 2. (The virtual photon may here also symbolize a general electroweak exchange of W and γ/Z bosons.) The matrix elements [7] are, for each given x and Q^2, complicated functions of three (Lorentz invariant) variables. These variables correspond to the new degrees of freedom in terms of, e.g., the relative sharing of energy between the two scattered partons, the opening angle between them, and an azimuthal angle with respect to the scattered lepton direction Although the azimuthal dependence can often be neglected to first approximation, it is included for completeness in our treatment. The matrix elements are divergent in the limit when the gluon energy or the opening angle vanishes (soft or collinear singularities). These divergences are partly cancelled by virtual corrections to the lowest order graph, and partly absorbed in the Q^2-dependent structure functions.

For convenient Monte Carlo simulation of events, it is necessary to impose a cutoff on the singular regions of the first order matrix elements. This can be done

Fig. 3. Schematic drawing of the QCD branching processes in initial and final state radiation. (The lines with momenta p symbolize partons in general, i.e. quarks and gluons.)

e.g. by requiring a minimum invariant mass m_{cut} between any pair of partons in the hadronic final state (with the target remnant system counted as one parton). From a physical point of view, it would be natural to assume m_{cut} independent of W. However, with increasing W the first order processes would then ultimately obtain a probability larger than unity. It is therefore necessary to allow for some variation in m_{cut} as a function of W (and x). The complete electroweak scattering cross section, exact first order QCD matrix elements and target remnant treatment are implemented in a Monte Carlo event generator [8] which has been used for the results in this paper. The EHLQ set 1 structure functions [9] have been used throughout, but we note that our results are not sensitively dependent on the specific structure function parametrization used.

An alternative to matrix elements is provided by parton showers, schematically illustrated in fig. 3. In the parton shower approach a number of interference effects are neglected. In particular, there is an arbitrary separation of radiation into an initial state cascade and a final state one. Both of these showers can be described as a successive application of the three basic branchings q → qg, g → gg and g → q$\bar{q}$, as described by the Altarelli-Parisi equations [10]. The details are different, however. The initial state shower is a spacelike one: there is a main branch of the cascade, stretching from the shower initiator up to the parton at the hard interaction, along which parton virtualities are increasingly spacelike ($Q_5^2 < Q_3^2 < Q_1^2$ in fig. 3, where $Q_i^2 = -m_i^2 > 0$). Only the side branches (partons 2 and 4 in fig. 3) may be on

mass-shell or timelike. The final state shower, on the other hand, is a timelike one, i.e. all partons have $m^2 \geqslant 0$, and virtualities decrease at each branching. A cutoff, typically $m_0^2 = Q_0^2 = 1$ GeV^2, is used to limit the emission of soft and collinear partons. Contrary to the matrix element alternative, there is no need (or motivation) for introducing an energy dependence in this cut. The models for initial and final state showers in leptoproduction are presented in [11] together with some general results.

The final state shower approach has been extensively studied in e^+e^- annihilation at PETRA/PEP energies. It is well developed, with soft gluon interference effects taken into account [12], leading to a good agreement with the data. We use the algorithm in [13,14]. The initial state shower algorithms are less mature, but have nevertheless proven phenomenologically relevant in high-$p_\perp$ p$\bar{\text{p}}$ collider events. The backwards evolution scheme of [15,16] is here employed. The initial state radiation contribution to gluon emission is less extensive than that from final state one, as a combined effect of phase space differences and a structure function related suppression of initial state radiation. Some new problems arise when shower models are to be used for deep inelastic scattering. In order that the shower algorithm leave kinematical variables unchanged, as defined by the scattered lepton, additional constraints must be taken into account [11].

It is furthermore ambiguous as to what sets the scale for the maximum virtuality in the shower. The natural alternatives here are Q^2 and W^2 (or more generally a function of these two variables). A good scheme for matching on to the exact first order matrix elements for deep inelastic scattering, which could resolve this, is still lacking. We note that, although Q^2 is the fundamental parameter in the matrix elements, the x-dependent factors make the basic transverse momentum properties depend mainly on W^2 (for not too small x) [7]. One way to study the effects of the different possibilities is shown in fig. 4, where average summed $E_\perp$ of partons is plotted as a function of W for different fixed Q^2 values. For reasonably large Q^2, PS with either Q^2 or W^2 (properly speaking $W^2/4$ [11]) as maximum virtuality then agree with the ME result (considering that the ME approach does not include the soft gluon region covered by the PS one), whereas for $Q^2 \ll W^2$ (x small) the use of Q^2 as scale would seem preferable, if the ME results are used as guideline. This is only half of the story, however: even with $Q^2 \ll W^2$ the ME approach does contain a tail of high-$p_\perp$ jets, which is entirely absent with an abrupt PS cutoff at virtuality Q^2. In a Monte Carlo approach, it would therefore be preferable to use W^2 as scale, but then apply rejection techniques to match on to the hard emission matrix element results. Based on these considerations we choose to use W^2 for the maximum virtuality, but note that our results are not very sensitive to this choice since we impose cuts that avoid the problematic low-x region. In the spirit of the leading log approximation, one would then expect soft and collinear gluon emission to be well described by parton showers, whereas the amount of hard radiation is somewhat uncertain.
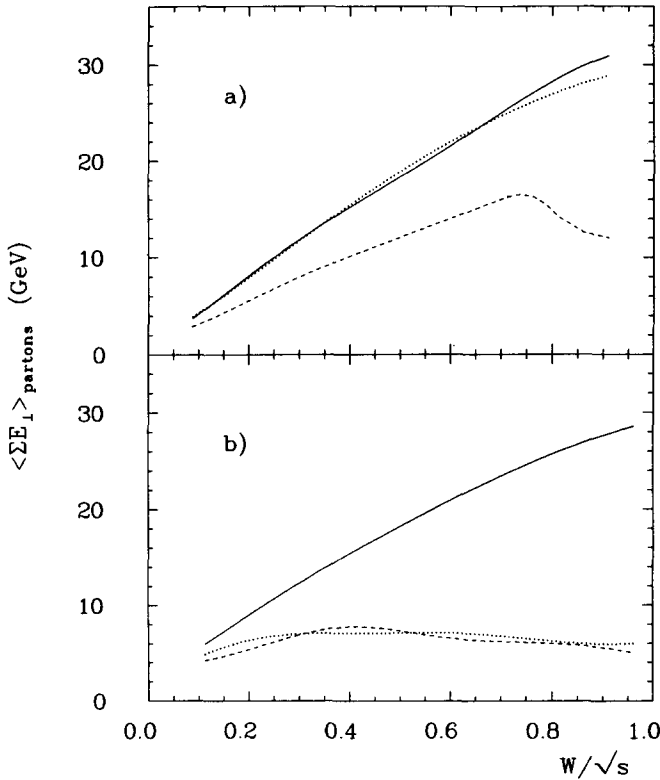
Fig. 4. Average summed transverse energy of partons, $\langle \Sigma E_{\perp} \rangle$, as a function of $W/\sqrt{s}$ at HERA energy for (a) $Q^2 = 10^4$ GeV^2 ($Q^2/s = 0.1$) and (b) $Q^2 = 100$ GeV^2 ($Q^2/s = 0.001$). Parton shower (PS) with maximum virtuality W^2 (full line), with Q^2 (dotted line) and for first order matrix elements (ME) (dashed line).

Once the parton configuration of a leptoproduction event has been specified, by matrix elements or parton showers, the fragmentation of these partons can be described, e.g., by the Lund string fragmentation model [1,14]. In the simplest case, valence quark scattering without gluon emission, a string is stretched between the scattered quark and the remnant diquark. For more complicated events there may be one or more strings, each corresponding to a colour singlet subsystem. Each string is stretched between a quark end and an antiquark or diquark one, with gluons appearing as energy and momentum carrying kinks on these strings. In first order matrix elements and leading log shower evolution alike, the way the strings should be stretched between the scattered partons (i.e. their colour ordering) is unambiguous; problems would arise with exact second order matrix elements, however.

The treatment of the hadron remnant system is not unique, except possibly when a valence quark is "kicked out" of the incoming hadron, leaving behind a diquark

system. For processes which give a more complex remnant, phenomenological recipies must be employed [17]. In the boson-gluon fusion process (or a parton shower initiated by a gluon), the colour octet qqq-remnant is subdivided into a colour triplet quark and an antitriplet diquark, sharing the available energy according to an assumed distribution, and connected by two independent strings to the produced antiquark and quark, respectively. Correspondingly, if a sea antiquark (quark) is kicked out of a nucleon, the remaining qqqq (qqq$\bar{\text{q}}$) system, which contains the partner quark (antiquark) to the struck one, is divided into a baryon plus a quark (a meson plus a diquark); the latter is connected with a string to the struck quark. Sensible recipes are here included in the Monte Carlo descriptions.

3. Comparisons with present data

The natural testing ground for a model is, of course, comparisons with experimental data. In this section we focus on recent results from the European Muon Collaboration [18], which provide an update of previous studies [6]. In these papers, results for different variations of the basic Lund model for deep inelastic scattering [19] are also presented. It is concluded that good agreement with the data can be obtained if both hard first order QCD processes (matrix elements) and soft gluon radiation (in an approximate resummation treatment [3]) are included, but not if either of these components is absent. In this section, we therefore emphasize the comparisons with the new parton shower alternative, which is an attempt to describe both hard and soft perturbative QCD radiation within the same framework. As will be seen, a qualitatively good agreement is obtained, but with some visible quantitative differences. These are most likely real but, while the EMC data are corrected for detector imperfections, residual differences could be present compared to our Monte Carlo event simulation, which only take the overall kinematical cuts into account, i.e.

$$Q^2 > 4 \text{ GeV}^2, \qquad 4 < W < 20 \text{ GeV}, \qquad 20 < \nu < 260 \text{ GeV},$$

$$E_{\mu'} > 20 \text{ GeV}, \qquad y < 0.9, \qquad \theta_\mu > 0.75^\circ. \tag{5}$$

In fig. 5 is shown the average $p_\perp^2$ w.r.t. the current direction as a function of $x_F = 2p_z/W$ (in the hadronic CM frame). This is a measure of the activity separately for the forward and backward regions. In the parton shower language, the increased forward activity is a result of final state radiation being more extensive than initial state one, enhanced by a tendency of initial state radiation to be more central. In the backward region, the main $p_\perp$ contribution therefore comes from fragmentation $p_\perp$ and primordial transverse momentum, $k_\perp$. The fragmentation $p_\perp$ used here is given by a gaussian in p_x and p_y separately, with $\sigma = 0.40$ GeV, to be compared with the standard e^+e^- values 0.35 GeV for parton showers and 0.40
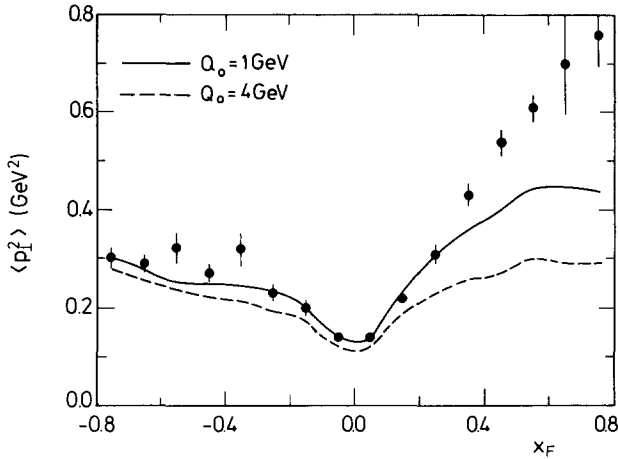
Fig. 5. Average $p_\perp^2$ as a function of $x_F = 2p_z/W$ in the hadronic CM frame. PS with cutoff mass 1 GeV (full line) and 4 GeV (dashed line); data from EMC [18].

GeV for matrix elements. The primordial $k_\perp$, which is treated by a similar gaussian, has $\sigma = 0.44$ GeV, corresponding to a reasonable Fermi motion. For large positive x_F, however, QCD contributions are important. With a 4 GeV parton shower cutoff mass, the model is here far below the data, as is the matrix element alternative without soft gluon radiation [6, 18]. If instead the standard cutoff mass, 1 GeV, is used, the extra emission of soft gluons in the shower leads to a significant increase of $\langle p_\perp^2 \rangle$ at large x_F, although not enough to explain the data. It is very difficult to increase the model results in this region, by changing available parameters within reasonable limits, without destroying the good agreement in other regions and variables. An increase of Λ to 0.8 GeV can give agreement out to $x_F \approx 0.55$, but would eventually have a $\langle p_\perp^2 \rangle$ decreasing with x_F, as a fairly straightforward consequence of the limited phase space for gluon emission in this region. An increase of primordial $k_\perp$ could give the desired effect in the forward region, but would then give too large an effect in the backwards direction (cf. ref. [18]). We note, however, that the systematic errors on the data (not shown) are not insignificant in this region, but presumably of a magnitude similar to the statistical ones. Such errors would, furthermore, normally lead to an overestimate compared to the true values.

In contrast to e^+e^- physics, leptoproduction events contain a well-defined event axis given by the virtual boson direction. Therefore, a detailed insight into the effects of primordial $k_\perp$ and soft gluons may be found by studying the details of transverse momentum compensation, as suggested in ref. [3]. In the EMC analysis [18], a leading forward trigger particle is defined by the requirement $x_F > 0.5$, and a leading backward one by $-0.5 < x_F < -0.2$ (i.e. excluding the extreme backward

region where acceptance is worse). The $p_\perp$-weighted rapidity spectrum of the trigger particle in the hadronic CM frame is then defined by

$$\frac{\mathrm{d}P_\perp^{\mathrm{trig}}}{\mathrm{d}y^*} = \frac{1}{N_{\mathrm{ev}}} \int p_\perp \frac{\mathrm{d}^2 N^{\mathrm{trig}}}{\mathrm{d}p_\perp \, \mathrm{d}y^*} \mathrm{d}p_\perp , \qquad (6)$$

where N^{trig} is the number of trigger particles, and a balancing transverse momentum flow by

$$\frac{\mathrm{d}P_\perp^{\mathrm{bal}}}{\mathrm{d}y^*} = \frac{1}{N_{\mathrm{ev}}} \int p_\perp' \frac{\mathrm{d}^2 N^{\mathrm{bal}}}{\mathrm{d}p_\perp' \, \mathrm{d}y^*} \mathrm{d}p_\perp' . \qquad (7)$$

Here $p_\perp' = p_\perp \cos\phi$, where ϕ is the azimuthal angle around the virtual photon direction with $\phi = 0$ being defined by the trigger particle. The trigger particle spectra, fig. 6a, are very much constrained by the average $p_\perp^2$ in these x_F bins, earlier shown in fig. 5, and consequently a good agreement exists. The rapidity spectra for the balancing particles, shown in fig. 6b and 6c, are nontrivial. For example, a large primordial $k_\perp$ would lead to a strong maximum around $y^* = -2$ for the $p_\perp$ compensation of a forward particle [3,18]. Also, the effects of fairly soft gluon emission are crucial for a reasonable agreement, as is shown by the difference between the results for 1 and 4 GeV cutoff masses in the showers.

In fig. 7 is shown the sum of all final state hadron $p_\perp^2$ in and out of an event plane, which contains the current direction q and is rotated (around the current axis) so as to minimize $\Sigma p_{\perp\,\mathrm{out}}^2$, i.e. a kind of sphericity orientation. The long tail in the $\Sigma p_{\perp\,\mathrm{in}}^2$ distribution again emphasizes the importance of gluon emission effects, but this time predominantly of fairly hard gluons, which (in this aspect) are here seen to be well modelled by the parton shower.

The charged particle multiplicity is a simple event measure (although not trivially measured) with a surprisingly rich structure. In a recent EMC study [20], multiplicity distributions are shown to agree well either with a positive binomial, a poissonian or a negative binomial, depending on the total energy W and the rapidity window used. At all energies, however, the deviations from a simple poissonian are small. In table 1 a comparison is presented with the data for average multiplicity and the $1/k$ value in the full rapidity range. It should be noted that the model calculations involve no explicit fitting to a given shape, but only derive the $1/k$ value from the relation $(\sigma/\bar{n})^2 = 1/\bar{n} + 1/k$, with $1/k = 0$ for a poissonian, < 0 for a positive binomial and > 0 for a negative one.

At EMC energies, the evolution of $\langle n_{\mathrm{ch}} \rangle$ with W provides no discrimination between the QPM and the PS alternatives: either gives a reasonable, but not good, description of data, table 1. In these figures, K_S^0, Λ, $\bar{\Lambda}$ and Dalitz π^0 decays are excluded. If this is not done, multiplicities are almost 10% higher. Since the multiplicity is affected by most aspects of the perturbative QCD and fragmentation
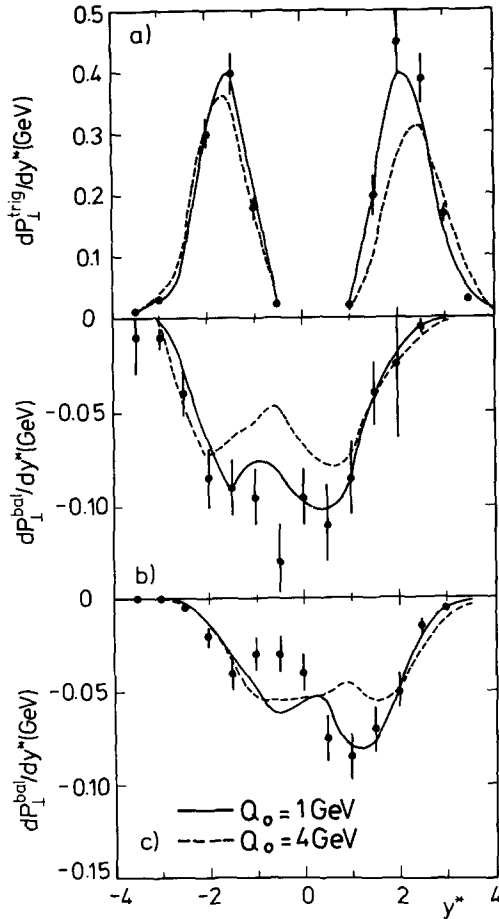
Fig. 6. Rapidity distribution, $\mathrm{d}P_\perp^{\mathrm{trig}}/\mathrm{d}y^*$ (eq. (6)), for trigger particles with $x_F > 0.5$ and $-0.5 < x_F < -0.2$: (a) Rapidity distribution, $\mathrm{d}P_\perp^{\mathrm{bal}}/\mathrm{d}y^*$ (eq. (7)), of the transverse momentum balancing the (b) forward and (c) backward trigger particle. PS with cutoff mass 1 GeV (full line) and 4 GeV (dashed line); data from EMC [6,18].

process, several parameters of the model could be used to shift the results by small amounts. Had not the preferred fragmentation $p_\perp$ value been changed from 0.35 to 0.4 GeV (without a corresponding returning of longitudinal fragmentation parameters), $\langle n_{\mathrm{ch}} \rangle$ would have been up to 0.3 units higher (for the larger W values). A change of the Λ parameter in the parton shower, from 0.4 to 0.3 GeV, would have given almost as large a reduction. By comparison, the dependence on the details of the target remnant treatment is smaller: rather drastic variations give less than ± 0.1 units of change.

The results for $1/k$ follow the W evolution of the data very well. The model curves are systematically more narrow, however, by about 0.025 units in $1/k$. This is
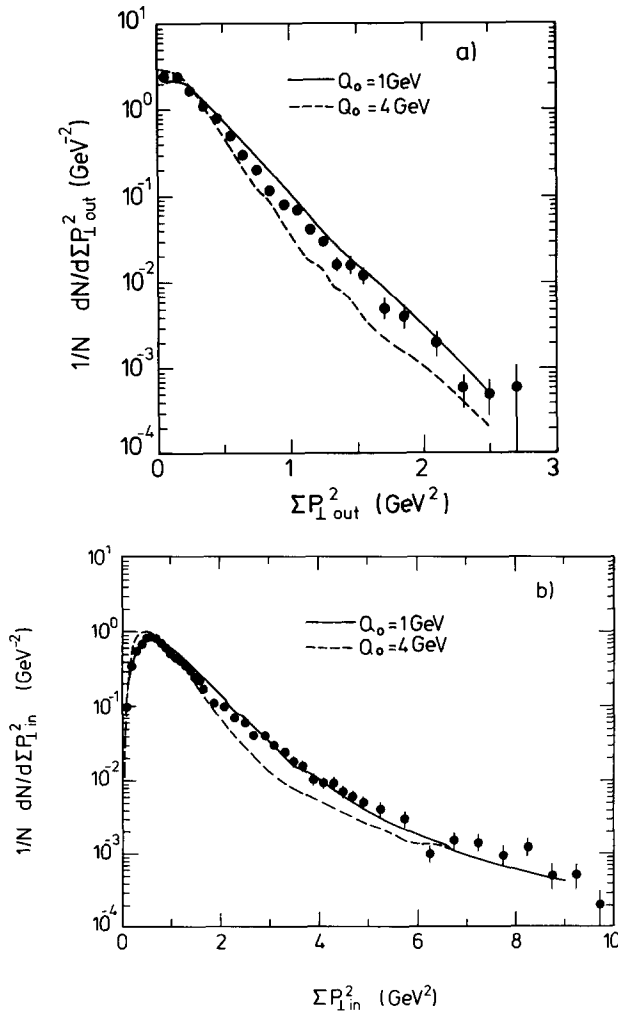
Fig. 7. Distribution of summed transverse momentum-squared in the event (a) out of and (b) within an event plane chosen so as to minimize $\Sigma p^2_{\perp \, out}$. PS with cutoff mass 1 GeV (full line) and 4 GeV (dashed line); data from EMC [18].

true both without and with showers: in the energy range considered here the increased width caused by gluon emission is balanced by the increased average multiplicity. It may be somewhat surprising that also the QPM gives distributions almost as broad as poissonian ones. The reason here is that the presence of a hadronic beam remnant gives a reduction of the average multiplicity, compared to the case of an antiquark remnant (e^+e^- events or pion target), without a corresponding reduction in width. At small energies this effect is overshadowed by a general narrowing simply from energy conservation effects.

TABLE 1
Average charged multiplicity and the $1/k$ parameter for different W bins

W (GeV)	data		QPM		PS	
	$\langle n_{ch}\rangle$	$1/k$	$\langle n_{ch}\rangle$	$1/k$	$\langle n_{ch}\rangle$	$1/k$
4–6	4.08	−0.058	3.81	−0.087	3.78	−0.088
6–8	4.89	−0.034	4.44	−0.062	4.44	−0.067
8–10	5.55	−0.018	5.06	−0.042	5.14	−0.053
10–12	6.09	−0.013	5.67	−0.032	5.72	−0.038
12–14	6.51	−0.002	6.05	−0.027	6.31	−0.030
14–16	6.85	0.003	6.52	−0.019	6.74	−0.024
16–18	7.20	0.007	6.86	−0.020	7.21	−0.017
18–20	7.48	0.017	7.14	−0.010	7.57	−0.010

k is defined by $(\sigma/\langle n_{ch}\rangle)^2 = 1/\langle n_{ch}\rangle + 1/k$, where σ is the dispersion. Quark-parton model and parton shower model compared with EMC data [20].

The EMC analysis also contains information on multiplicities separately in the forward and backward hemisphere, and in rapidity windows. Here particle identification is important, since masses enter explicitly in the boost from the lab frame to the hadronic CM frame. As an example, the bin $18 < W < 20$ GeV would give a backward hemisphere multiplicity of 3.14 if correct masses are used, 2.80 if all particles are assumed massless, and 3.45 if twice the pion mass (i.e. an "average charged mass") is used. The EMC Collaboration can only identify approximately 50% of the tracks, and then make various assumptions for the rest [20]. In comparison with the data, the PS results are consistently 0.3 units too low in the backward hemisphere, with the QPM results even lower, table 2. As a consequence, the models are above the data in the forward hemisphere. In summary, multiplicities are not good probes of QCD properties at EMC energies, since so much of the

TABLE 2
Average charged multiplicity in the forward (current) and backward hemispheres
for the QPM and PS models compared to EMC data [20]

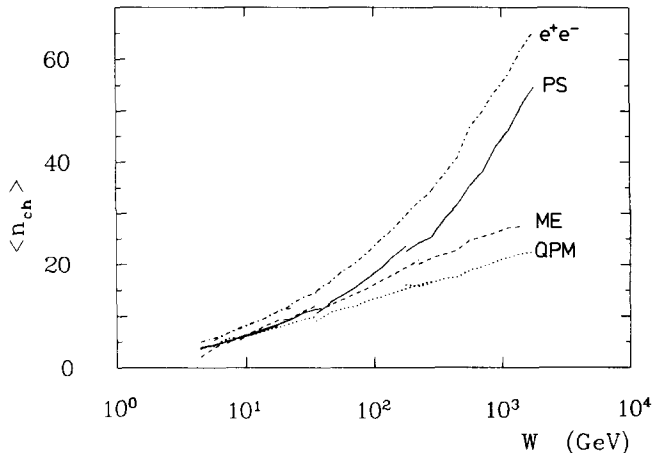| W (GeV)	n_{ch} forward			n_{ch} backward		
	data	QPM	PS	data	QPM	PS
4–6	2.10	2.22	2.25	1.85	1.59	1.52
6–8	2.60	2.59	2.63	2.14	1.84	1.81
8–10	3.01	3.00	3.03	2.46	2.06	2.11
10–12	3.26	3.36	3.39	2.71	2.31	2.34
12–14	3.55	3.58	3.73	2.83	2.47	2.58
14–16	3.65	3.83	3.98	3.03	2.69	2.77
16–18	3.88	4.00	4.24	3.28	2.86	2.97
18–20	3.96	4.15	4.42	3.49	2.99	3.14

Fig. 8. Average charged multiplicity as a function of W for QPM (dotted), ME (dashed) and PS (full). All curves are for neutral current events and exclude the scattered lepton; leftmost SPS, thereafter FNAL, HERA and LEP + LHC. For comparison, the same curve is shown for e^+e^- events using parton showers (dashed-dotted).

results obtained depend on details of the model and the analysis, present already with the QPM.

4. Event properties at higher energies

While the QPM fails to describe event properties already at present energies, either the ME or the PS option give a reasonable description of the data. Some $p_\perp$ quantities do, however, require the inclusion of soft gluon effects in the ME approach, i.e. a step towards the PS one. At higher energies the difference between the approaches is expected to increase, but in going from the SPS to the FNAL muon beam the increase in $\sqrt{s}$ from 23 to around 37 GeV is not big enough to show them clearly. At HERA, with $\sqrt{s} = 314$ GeV, or a possible combination of LEP and LHC, with $\sqrt{s} = 1.8$ TeV, the ME and PS results will differ substantially in some aspects. However, since the main difference between ME and PS is the lack of extra soft jets in the former description, the overall event shapes should still show a large similarity.

The most easily observed consequence of soft gluon emission is a faster increase of multiplicity with W, fig. 8. This statement is, however, strongly coupled to the choice of fragmentation parameters; it is always possible to make up for some of the effects of soft gluons by an explicit softening of the fragmentation spectrum (but not to change the basic $\ln W$ increase of $\langle n_{ch} \rangle$). The fragmentation parameters used for the ME approach have been determined by comparison with e^+e^- annihilation data, for an effective cutoff mass of roughly 4 GeV applied to the order α_s^2 matrix elements. If larger cutoff masses are used in leptoproduction, as becomes necessary
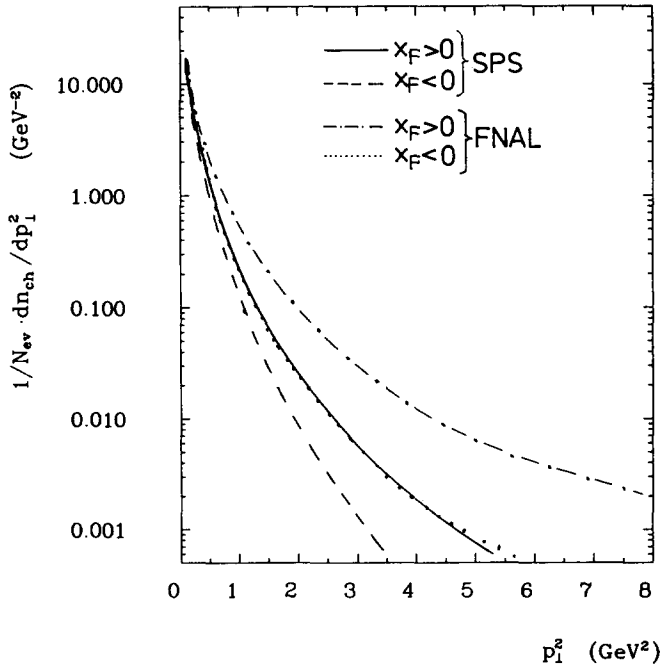
Fig. 9. Inclusive $p_\perp^2$ distribution in forward and backward hemisphere for SPS, 280 GeV μp, and FNAL, 750 GeV μp, interactions using the kinematical cuts defined for EMC (eq. (5)). Full line SPS forward, dashed SPS backward, dash-dotted FNAL forward and dotted FNAL backward.

when W is large, it would be allowed (but inconvenient) to retune the parameters accordingly. No corresponding excuse exists for the PS alternative; parameters determined in e^+e^- annihilation with the cutoff mass 1 GeV should also be valid for leptoproduction at all energies, as long as the same cutoff and Λ are used. The strong increase in multiplicity with the inclusion of multiple gluon emission is evident in fig. 8, but we note that the multiplicity in leptoproduction is still significantly lower than in e^+e^- annihilation events at the same energy. The reason for this is partly related to the reduced initial state radiation as compared to final state radiation (see sect. 2) and partly to the different fragmentation properties of the target remnant (diquark) as compared to normal quark hadronization.

The increase of the QCD effects from SPS to Fermilab fixed target energies is illustrated by the inclusive $p_\perp^2$ distribution in fig. 9. As noted before, the largest effect is concentrated in the forward region, although a significant increase in the backward target fragmentation region is also obtained. The ME results (not shown) are still similar to the PS ones; yet higher energies are required to clearly show the higher order effects in the PS approach in such inclusive variables.

For the following studies of ep collider physics, we normally use neutral current event samples (with full γ/Z^0 structure) defined by lower cuts in Q^2 and W^2,
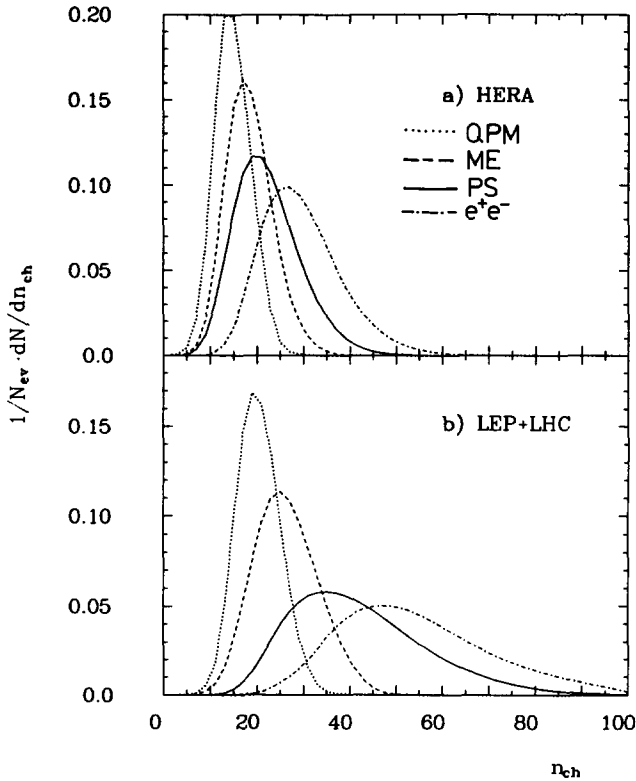
Fig. 10. Charged multiplicity distributions for neutral current events (a) for HERA events with $W = 163$ GeV and (b) for LEP + LHC ones with $W = 934$ GeV ($x = 0.1$, $y = 0.3$). QPM dotted, ME dashed, PS full, e^+e^- events of same energy dash-dotted.

in order to concentrate on the new and interesting region. For HERA the cuts are Q^2, $W^2 > 10^3$ GeV^2 and for LEP + LHC Q^2, $W^2 > 3 \times 10^4$ GeV^2. This amounts to having these variables larger than $\approx 1\%$ of the maximum possible, and the resulting cross-section in the standard model is 215 and 12 pb, respectively, leading to useful event samples with realistic luminosities. For some observables the influence of varying kinematics is not desirable, since that washes out the interesting effects. In such cases we fix the kinematics at $x = 0.1$, $y = 0.3$, which are approximately the mean values in the regions defined above. At HERA this corresponds to $Q^2 = 2950$ GeV^2 and $W = 163$ GeV, at LEP + LHC to $Q^2 = 96\,900$ GeV^2 and $W = 934$ GeV. Since our objective is to study the hadronic final state, the scattered lepton is never included in the following studies.

The charged multiplicity distributions are shown in fig. 10 for events with fixed kinematics. Note that not only the mean values $\langle n_{ch} \rangle$ are increased when going from QPM to ME to PS events, but even more so the width, i.e. the distributions

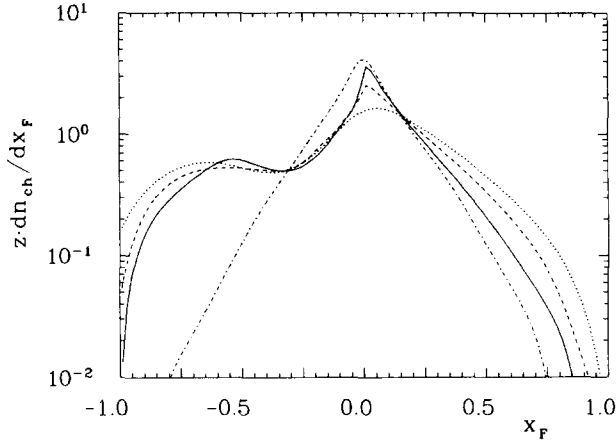Fig. 11. Energy-weighted distribution of longitudinal momenta, $z \, dn_{ch}/dx_F$, for charged particles in the hadronic CM frame of HERA events with Q^2, $W^2 > 10^3$ GeV^2 ($x_F > 0$ for the current jet and < 0 for the beam one). QPM dotted, ME dashed, PS full, e^+e^- events of same energy dash-dotted.

become increasingly non-poissonian. At these energies, already the QPM distribution is wider than a poissonian, as a consequence of the hadron remnant (cf. sect. 3). e^+e^- events, simulated with the same final state parton shower algorithm and at the same energies, show even larger multiplicities and fluctuations.

The importance of the baryon produced in the target region has already been noted [3]; see also ref. [21] for the basically good agreement of the model and EMC data on baryon x_F spectra. This importance is not an effect that disappears with increasing energy, see fig. 11 for the z-weighted x_F-spectrum of charged particles ($z = 2E/W$, $x_F = 2p_z/W$ in the hadronic CM frame). The rapidity distributions in the hadronic CM frame, fig. 12, not only show the unequal fragmentation regions but also that QCD radiation predominantly occurs in the forward region (also the $\langle p_\perp \rangle$ values are significantly larger there).

In order to characterize event shapes, table 3 gives the mean values of $\langle S_{lin} \rangle$, $\langle A_{lin} \rangle$ (linear sphericity and aplanarity measures) and $\langle n_{jet} \rangle$ (using LUSPHE and LUCLUS in [14]) for charged particles. Here $\langle S_{lin} \rangle$ gauges the general level of non-twojetness, while $\langle A_{lin} \rangle$ measures the activity out of the event plane, and thus only receives parton level contributions from four-jets and onwards. While the ME and PS show a similar behaviour in the former quantity, PS are bound to give a much larger $\langle A_{lin} \rangle$ at large energies. The number of reconstructed jets tells a similar story as $\langle A_{lin} \rangle$ does. Again note the strong forward-backward asymmetry in jet activity.

The angular energy flow is defined as the energy-weighted cross-section, as a function of the parton/hadron polar angle w.r.t. the current axis in the hadronic CM frame. It has been suggested as an interesting observable, which reveals properties of the perturbative QCD matrix elements, see [3] and references therein.
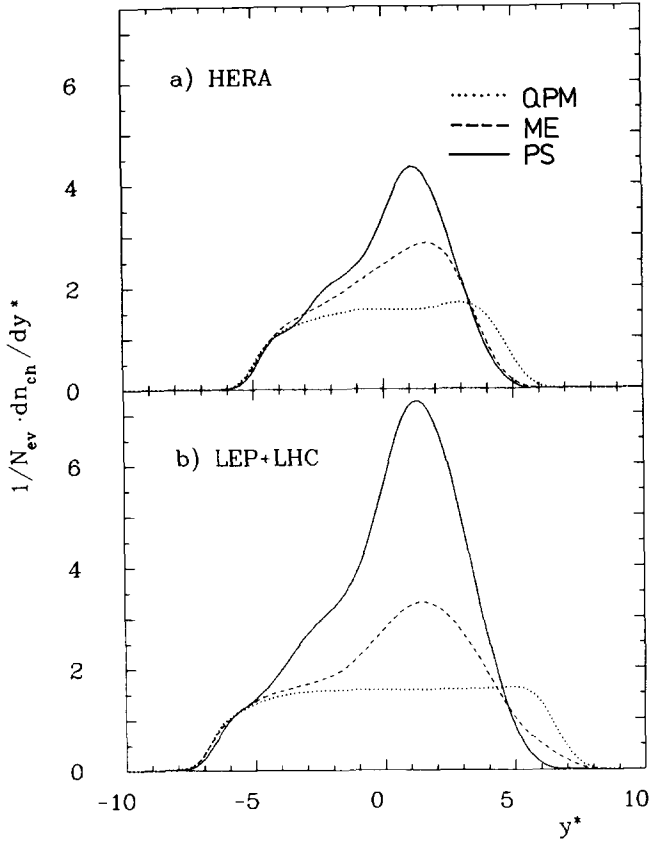
Fig. 12. Charged particle rapidity distribution, $(1/N_{ev})\,dn_{ch}/dy^*$, in the hadronic CM frame. (a) HERA events with Q^2, $W^2 > 10^3$ GeV^2 and (b) LEP + LHC ones with Q^2, $W^2 > 3 \times 10^4$ GeV^2. QPM dotted, ME dashed, PS full.

In QCD, radiated gluons tend to be along the scattered quark direction, thus producing a forward-backward asymmetry in the energy flow. We have, however, previously shown [3] that, at fixed target energies, this effect is almost completely washed out by the transverse energy flow produced by the dominating 2-jetlike events (quark + diquark jets) because of fragmentation $p_\perp$ and resonance decays. On the other hand, the unequal fragmentation properties of the forward quark and backward diquark lead to a larger asymmetry in the energy flow at fixed target energies. At HERA, these non-perturbative effects are expected to be less important, so that the measurable hadron energy flow should reveal the underlying parton level result from perturbative QCD. This is demonstrated in fig. 13. Although the 2-jet events (QPM, which essentially gives δ-functions at $\cos\theta = \pm 1$ at the parton level) still give a sizable hadron energy flow at large angles, it is smaller than that from QCD effects. It can also be seen that the PS result is less asymmetric

TABLE 3

Event shape properties of charged particles in the hadronic CM frame for HERA
with Q^2, $W^2 > 10^3$ GeV^2 and LEP + LHC with Q^2, $W^2 > 3 \times 10^4$ GeV^2

	$\langle S_{\text{lin}} \rangle$	$\langle A_{\text{lin}} \rangle$	$\langle n_{\text{jet}} \rangle$	asymmetry
HERA:				
QPM	0.033	0.010	1.98	0.02
ME	0.075	0.016	2.40	0.26
PS	0.104	0.026	2.79	0.47
e^+e^-	0.150	0.035	3.18	
LEP + LHC:				
QPM	0.006	0.002	2.01	0.00
ME	0.034	0.003	2.66	0.28
PS	0.062	0.011	4.58	1.13
e^+e^-	0.104	0.016	5.52	

Mean values of linear sphericity and aplanarity, number of reconstructed jets and the difference between number of jets in the forward (current) and backward hemisphere.

than the ME one, as a consequence of washout effects from the multigluon emission. Although the PS method involves approximations, this indicates that higher order effects tend to reduce the asymmetry calculated from first order QCD. This is more clearly seen in fig. 14, which shows the asymmetry defined by

$$A(\theta) = \frac{E(\theta) - E(\pi - \theta)}{E(\theta) + E(\pi - \theta)}, \qquad 0 < \theta < 90°, \qquad (8)$$

where $E(\theta)$ is the energy at polar angle θ. Also at HERA energies, the parton level asymmetry is significantly reduced by hadronization effects, as is clear from the comparison of the parton and hadron level result, but it remains large enough for experimental investigation of the basic QCD effect.

While the hadron CM frame is convenient for theoretical event studies, the boost from the lab frame to the hadronic CM frame does presuppose a knowledge of the event kinematics as well as hadron masses. Therefore studies in the lab frame have a certain interest. In terms of rapidity distributions, the beam jet looks the same, apart from an overall shift by $\ln[2(1 - x)|P|/W]$. The current jet is now fairly well compressed around the naive direction of the scattered quark, again with QPM giving the narrowest and PS the broadest distribution, fig. 15. (It should be noted, that even in the QPM model the energy and angle of the current jets are not exactly those expected from naive kinematics, due to the primordial $k_\perp$.) When different kinematical configurations are averaged over, the sharp dn/dy peak is smeared out, and what remains is a general increase in the "forward" region, where the current jets are to be found. In the QPM the resulting "forward-backward" asymmetry is
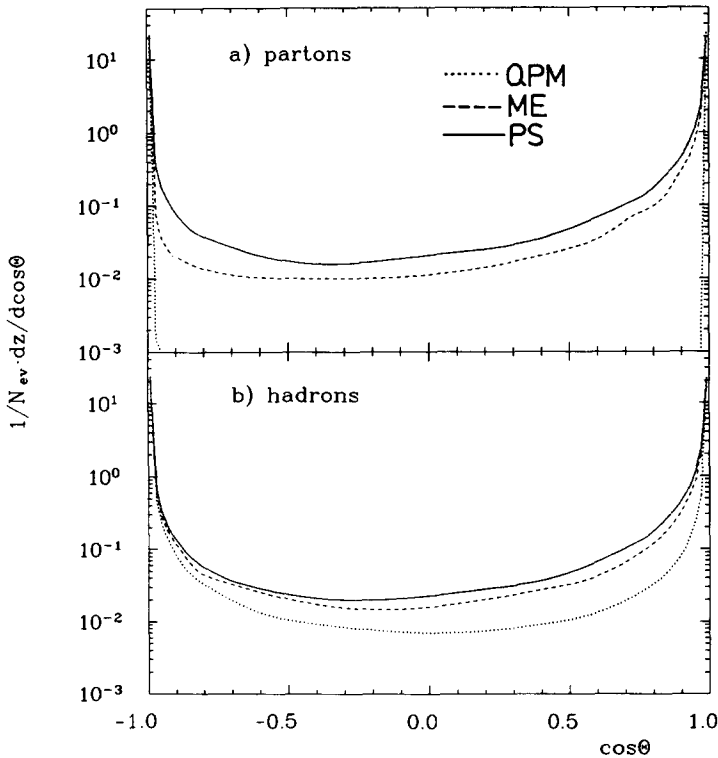
Fig. 13. Angular energy flow, $(1/N_{ev})\,dz/d\cos\theta$, where $z = E_h/W$ is the fractional hadron energy at angle θ, measured with respect to the current direction in the hadronic CM frame. HERA events with Q^2, $W^2 > 10^3$ GeV^2 (a) at parton level and (b) after hadronization. QPM dotted, ME dashed, PS full.

almost entirely kinematical in origin, whereas the ME and PS contain a further enhancement of the forward multiplicity from extra jet activity.

A broadening of jet width in azimuthal angle (around the beam axis), i.e. $dn/d\phi$, is also visible in a comparison between QPM, ME and PS. However, this broadening does not lead to significant changes 180° away from the scattered quark direction ($\lesssim$ factor 2). In particular, the isolation of the scattered electron is usually not worse because of the additional gluon radiation in PS compared to the ME case. A tiny class of events does appear, however, where the electron overlaps with a jet, which may make the electron energy measurement more difficult.

In e^+e^- annihilation, studies of the energy-energy correlation [22] have been useful as probes of the internal structure of jets [23]. In the hadronic CM frame, exactly the same analysis is easy to define. It is also possible to use a similar technique in the lab frame, as follows. For each event, denote by η_i, ϕ_i, $E_{\perp i}$ the pseudorapidity, azimuthal angle and transverse energy of particle i (or calorimeter cell i). Define a distance $\omega_{ij}^2 = (\eta_i - \eta_j)^2 + (\phi_i - \phi_j)^2$ in the $\eta - \phi$ space. With the
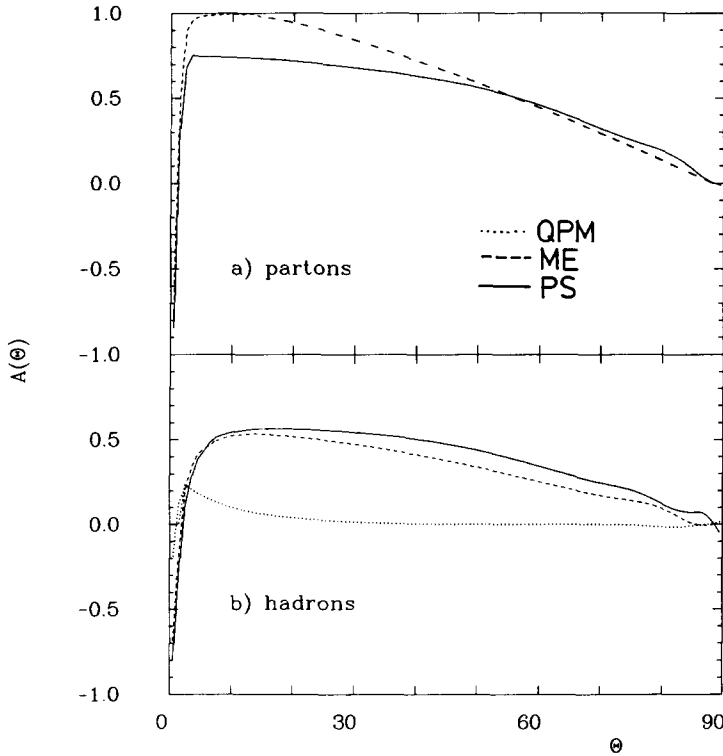
Fig. 14. Energy flow asymmetry, $A(\theta) = [E(\theta) - E(\pi - \theta)]/[E(\theta) + E(\pi - \theta)]$, as obtained from fig. 13. (Note the different horizontal scale compared to fig. 13.)

$k_\perp'^2 = Q^2(1 - y)$ of the scattered lepton as suitable normalization, the transverse energy-energy correlation at distance ω is then given by

$$\Omega(\omega) = \frac{1}{N_{\text{event}}} \sum_{\text{events}} \sum_{i \neq j} \frac{E_{\perp i} E_{\perp j}}{Q^2(1 - y)} \delta(\omega - \omega_{ij}) \qquad (9)$$

(where the δ function is smeared by the bin width used in histogramming). Note that the autocorrelation $i = j$ at the origin is not included here. The function $\Omega(\omega)$ is shown in fig. 16 for $\omega < 1$.

The three alternatives considered differ drastically in the predictions of $\Omega(\omega)$ on the parton level. In the QPM, only one jet is scattered, and $\Omega(\omega)$ is therefore vanishing. In the ME approach, $\Omega(\omega)$ is rather abruptly cut off for values smaller than $\omega \approx 0.4$. The presence of this central hole is a consequence of the invariant mass cuts imposed to stay away from the collinear singularity in the matrix
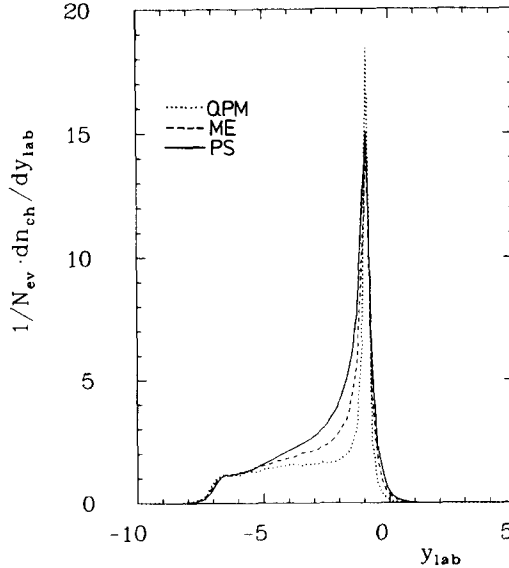
Fig. 15. Charged particle rapidity distribution, $(1/N_{ev}) \, dn_{ch}/dy$, in the lab frame for HERA events with $x = 0.1$, $y = 0.3$. QPM dotted, ME dashed, PS full.

elements. An approximate energy independence of the value $\omega \approx 0.4$ comes from the need to increase the mass cutoff as the energy is increased, in order to keep the probability for first order processes below unity. By contrast, parton showers are based on an energy-independent mass cutoff, and therefore the central hole shrinks with increasing energy.

Fragmentation effects tend to smear this picture; in particular the central hole is filled up by particle pairs coming from the same jet. Therefore no strong dip is present in the ME model for $\omega \approx 0.1$–0.4, as might have been expected. Only at LEP + LHC energies do the first signs of this appear (at $\omega \approx 0.3$). Already at HERA, however, there is a clear difference between the very narrow QPM distribution, the somewhat broader ME one and the rather broad PS one. Note that the difference between ME and PS indeed is a question of the "internal structure" of jets; for the wide angle region ($\omega > 1$, not shown) the two approach each other.

For an explicit jet reconstruction in the lab frame, it is again convenient to use the $(\eta, \phi, E_\perp)$ set of variables, here in a jet finding algorithm of the generic UA1 type (LUCELL in ref. [14]). In the algorithm, the transverse energy in all cells within a distance $\omega < \omega_{max}$ around an "initiator" cell are summed up, and if the $\Sigma E_\perp > E_{\perp \, min}$ for some threshold transverse jet energy $E_{\perp \, min}$, these cells together define one jet. In the following, typically $E_{\perp \, min} = 5$ GeV and $\omega_{max} = 0.5$ will be used. It should be pointed out that this kind of procedure is very convenient and natural in events where the current jet is reasonably central, but it may need to be
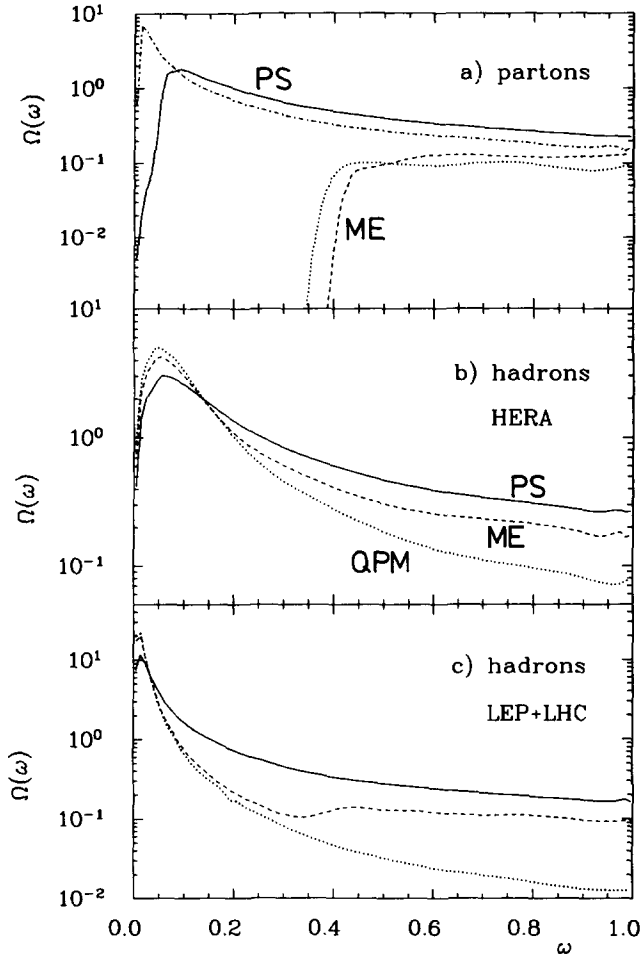
Fig. 16. Transverse energy correlation function $\Omega(\omega)$, eq. (9), for events with $x = 0.1$, $y = 0.3$. (a) parton level results for HERA, ME (dashed line) and PS (full), and LEP + LHC, ME (dotted) and PS (dash-dotted). (b) After hadronization at HERA, QPM (dotted), ME (dashed), PS (full). (c) After hadronization at LEP + LHC, notation as in (b).

modified for a search of very forward current jets. A separate study of this is in progress [24]. (There is also no built-in symmetry between finding jets resulting from initial and from final state radiation; for that, analyses in the hadronic CM frame are preferable.) For the following jet studies we have therefore chosen the fixed kinematics configuration which for HERA means a naive current jet at 44° from the proton beam direction, and for LEP + LHC at 25°.

Resulting jet multiplicity distributions are shown in fig. 17. The probability that more than one jet is found in the QPM case is exceedingly small, while several jets are found frequently with ME and PS. One jet is here usually fairly hard, and is to
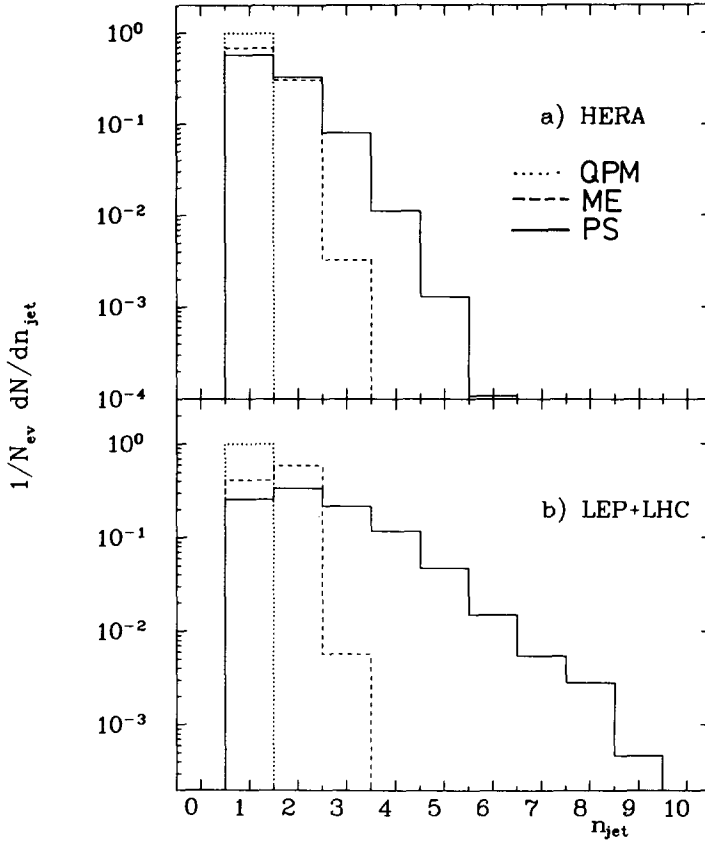
Fig. 17. Multiplicity distribution of reconstructed jets, (a) for HERA events, (b) for LEP + LHC ones, both with $x = 0.1$, $y = 0.3$. QPM dotted, ME dashed, PS full.

be found close to the naive current jet direction, whereas the softer jets are predominantly found shifted towards the beam jet direction, but still at fairly central rapidities. This is shown by the pseudorapidity distribution $dn_{jet}/d\eta$ for the reconstructed jet directions in fig. 18. Note that, while a very few jets are to be found closer to the target jet region with ME or PS than with QPM, most of the increased jet activity from higher order QCD is to be found in the same region as the current jets. This observation, also true in an event sample with varying kinematics, is not entirely trivial, since the kinematically allowed η range of emission is larger for the "extra" lower-energy jets. The number of jets found is obviously a function of the algorithm parameters. In fig. 19 is shown the effects of varying ω_{max} from 0.1 to 2, while keeping $E_{\perp min} = 5$ GeV fixed. Again, parton shower events are seen to have a richer subjet structure than matrix element ones. For very small ω_{max}, the algorithm becomes sensitive to the "calorimeter" granularity and is therefore less reliable.
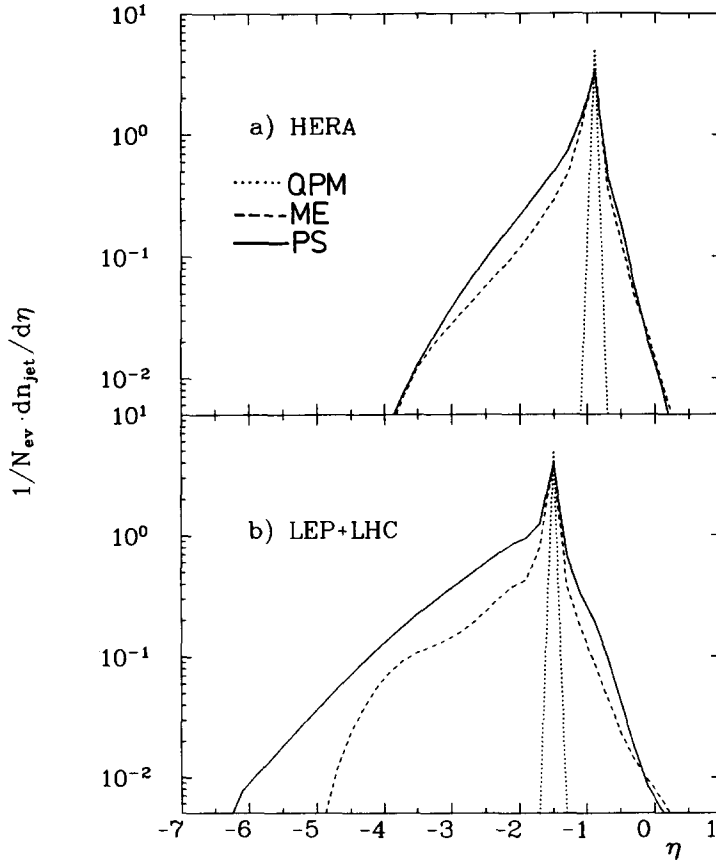
Fig. 18. Pseudorapidity distribution $(1/N_{ev}) \, dn_{jet}/d\eta$ of reconstructed jets, (a) for HERA events and (b) for LEP + LHC ones, both with $x = 0.1$, $y = 0.3$. QPM dotted, ME dashed, PS full.

5. Reconstruction of event kinematics

For most studies at future ep colliders a precise knowledge of the event kine-matics is of major importance; the structure function analyses, e.g., require differen-tial cross sections as functions of x and Q^2. As noted in the introduction, the kinematics is in principle straightforwardly obtained from the scattered lepton in neutral current events, whereas it has to be measured from the hadronic system in charged current interactions. In the naive QPM, the scattered quark gives the necessary information, but in reality a number of smearing effects enter, like fragmentation, mass effects and jet reconstruction algorithms. When QCD effects are included, the kinematics of the hard scattering is more complicated, since initial state radiation may give the struck quark a large virtuality and transverse momen-tum. In addition, final state radiation gives a set of partly separated jets, with total energy, direction and invariant mass difficult to determine.
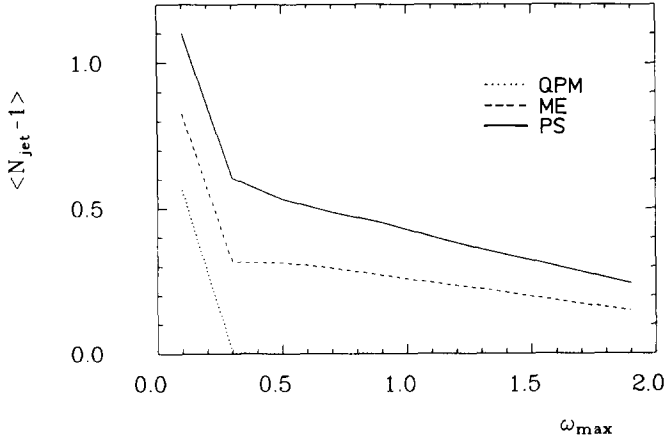
Fig. 19. Average number of reconstructed jets (subtracting one to account for the trivial current jet) as a function of jet cone opening angle ω_{max} in the jet finding algorithm, applied to HERA events with $x = 0.1$, $y = 0.3$. QPM dotted, ME dashed, PS full.

Thus, it is important that the kinematics reconstruction does not rely on finding individual jets in the final state, which should instead be regarded as a single system whose internal structure is not of importance. This is the essence of the "Jacquet-Blondel" method [25] which is based on energy-momentum conservation between the invisible neutrino and the hadronic system. Letting p_H be the four-vector of the *complete* hadronic system, i.e. the vector sum of all hadrons, the experimentally useful relations are simply derived from the basic kinematics as follows

$$y = \frac{P \cdot q}{P \cdot k} = \frac{P \cdot (p_H - P)}{P \cdot k} = \frac{E_p(E_H - p_{zH})}{2E_e E_P} = \frac{E_H - p_{zH}}{2E_e} = \frac{\Sigma_h(E_h - p_{zh})}{2E_e} \quad (10)$$

$$Q^2 = \frac{k_{\perp}'^2}{1 - y} = \frac{p_{\perp H}^2}{1 - y} = \frac{[\Sigma_h p_{\perp h}]^2}{1 - y}. \quad (11)$$

The lepton and proton masses are here neglected and the incoming proton moving in the $+z$ direction. Clearly this method makes no assumption on the internal structure of the incoming proton nor of the final hadron system.

This method is particularly suitable since particles along the proton direction, which are likely to be lost in the beam pipe, have a minimal influence because of their small $E_h - p_{zh}$ and $p_{\perp h}$. Nevertheless, the ultimate accuracy is determined by these particle losses (as well as the lost neutrinos from heavy flavour decays). The resulting uncertainty in y and Q^2 is illustrated in fig. 20 for HERA and LEP + LHC. It is important to realise that the errors arise dominantly from kinematical configurations where the current jet is close to the beam pipe. The larger energy at
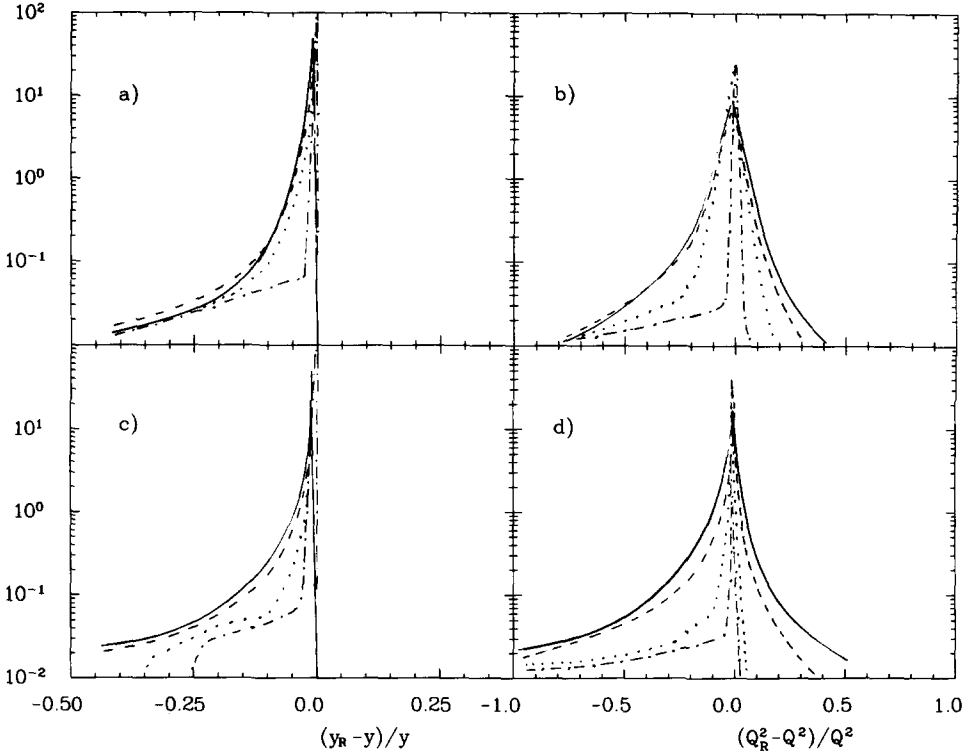
Fig. 20. Relative error on y and Q^2 reconstruction due to particle losses at HERA with Q^2, $W^2 > 10^3$ GeV^2, (a) and (b), and at LEP + LHC with Q^2, $W^2 > 3 \times 10^4$ GeV^2, (c) and (d). QPM with full angular coverage dash-dotted (tail due to neutrinos from charm etc. decays). With 70 mrad beam hole: QPM dotted, ME dashed, PS full.

LEP + LHC tend to give more collimated jets, which is an advantage in this respect. On the other hand, the larger energy ratio between the beams gives a larger boost that moves the current jet closer to the beam hole. Thus, the resulting reconstruction accuracy depends strongly on the kinematic region studied. In our example, the relative errors are similar as at HERA. Comparing the different models, the ME and PS results agree well, i.e. the extra soft gluon emission in parton showers do not contribute significantly to any extra smearing of the kinematics reconstruction. A use of the QPM, which totally neglects gluon radiation, would however paint too rosy a picture of the kinematics reconstruction problem.

Although the shifts arising in the kinematical variables through these effects can to a large extent be corrected for, it will influence the useful region where migration between different x, Q^2 bins are of a tolerable magnitude. Furthermore, it should be noted that the examples above are based on ideal detectors; only the limited coverage is taken into account. In the real world, extra sources of error arise through calorimeter imperfections and radiative corrections.

6. Summary

It has been known for a long time that the quark parton model description fails to account for a number of observed properties of leptoproduction events. A generally good description has been obtained with an approach based on first order matrix elements. There have been a few distributions, notably those for transverse momentum compensation, where agreement has not been entirely satisfactory. In order to understand these, soft gluon effects have been invoked and, with a simple soft gluon simulation scheme, good agreement with the data has indeed been obtained. In this paper we have shown that a parton shower approach is equally successful (except for a too low $\langle p_\perp^2 \rangle$ at larger x_F, fig. 5), and this without the need for an artificial separation into hard and soft radiation. (This may, of course, be considered as a post facto justification for our simple soft gluon summation scheme.) Good agreement is only obtained if the parton shower cutoffs are chosen fairly small, e.g. $m_0 = Q_0 = 1$ GeV, in agreement with experience from e^+e^- annihilation.

At HERA energies, results obtained with the quark parton model are entirely misleading, since QCD effects are very important for the structure of the hadronic system. For overall event properties, the approach based on first order QCD matrix elements and that of parton cascades show more agreement than might have been expected. Nonetheless, the higher order QCD effects included in parton showers give noticeable effects by making the events more "smeared": they have larger charged multiplicity, broader current and target jets, more signs of multijet structure, etc. A limitation of the matrix element approach here is that a fairly large cutoff is required to avoid the divergences, and thus keep the total probability for the first order QCD processes below unity. Despite the uncertainties present in the formulation of the parton shower alternative, it is therefore likely that the picture obtained here is also the more realistic one.

References

[1] B. Andersson, G. Gustafson, G. Ingelman and T. Sjöstrand, Phys. Reports 97 (1983) 31
[2] B. Andersson, G. Gustafson, G. Ingelman and T. Sjöstrand, Z. Phys. C9 (1981) 233
[3] G. Ingelman, B. Andersson, G. Gustafson and T. Sjöstrand, Nucl. Phys. B206 (1982) 239
[4] EMC Collaboration, J.J. Aubert et al., Phys. Lett. 95B (1980) 306, 100B (1981) 433
[5] T. Sjöstrand, Z. Physik C26 (1984) 93;
    JADE Collaboration, W. Bartel et al., Z. Phys. C25 (1984) 231, C33 (1986) 23;
    Mark II Collaboration, A. Petersen et al., Phys. Rev. Lett. 55 (1985) 1954, SLAC-PUB-4290/LBL-23243 (1987);
    S. Bethke, Heidelberg Habilitation thesis, LBL 50-208 (1987);
    T. Takahashi, Tokyo PhD thesis, UT-HE-87/2 (1987)
[6] EMC Collaboration, J.J. Aubert et al., Phys. Lett. 119B (1982) 233;
    EMC Collaboration, M. Arneodo et al., Phys. Lett. 149B (1984) 415
[7] G. Altarelli and G. Martinelli, Phys. Lett. 76B (1978) 89;
    A. Méndez, Nucl. Phys. B145 (1978) 199;
    R. Peccei and R. Rückl, Nucl. Phys. B162 (1980) 125;
    Ch. Rumpf, G. Kramer and J. Willrodt, Z. Phys. C7 (1981) 337

[8] G. Ingelman, LEPTO version 5.2, DESY preprint, in preparation

[9] E. Eichten, I. Hinchliffe, K. Lane and C. Quigg, Rev. Mod. Phys. 56 (1984) 579, 58 (1986) 1047

[10] G. Altarelli and G. Parisi, Nucl. Phys. B126 (1977) 298

[11] M. Bengtsson and T. Sjöstrand, LUTP 87-10 (1987)

[12] A.H. Mueller, Phys. Lett. 104B (1981) 161;
B.I. Ermolaev and V.S. Fadin, JETP Lett. 33 (1981) 269;
G. Marchesini and B.R. Webber, Nucl. Phys. B238 (1984) 1

[13] M. Bengtsson and T. Sjöstrand, Nucl. Phys. B289 (1987) 810

[14] T. Sjöstrand and M. Bengtsson, Computer Phys. Comm. 43 (1987) 367;
T. Sjöstrand, Computer Phys. Comm. 39 (1986) 347

[15] M. Bengtsson, T. Sjöstrand and M. van Zijl, Z. Phys. C32 (1986) 67

[16] H.-U. Bengtsson and T. Sjöstrand, Computer Phys Comm. 46 (1987) 43

[17] B. Andersson, G. Gustafson, G. Ingelman and T. Sjöstrand, Z. Phys. C13 (1982) 361

[18] EMC Collaboration, M. Arneodo et al., Z. Phys. C36 (1987) 527

[19] G. Ingelman, LEPTO version 4.3, CERN program pool long writeup, program W5046 (1986)

[20] EMC Collaboration, M. Arneodo et al., Z. Phys. C35 (1987) 335

[21] EMC Collaboration, M. Arneodo et al., Phys. Lett. 150B (1985) 458

[22] C. Basham, L. Brown, S. Ellis and S. Love, Phys. Rev. Lett. 41 (1978) 1585

[23] JADE Collaboration, W. Bartel et al., Z. Phys. C25 (1984) 231

[24] P. Burrows, G. Ingelman and E. Ros, DESY preprint 87-167, Z. Phys. C in press

[25] U. Almadi, ed., Proc. study of an ep facility for Europe, DESY 79/48 (1979) pp. 391–394